

COSMIC’s Large-Scale Search for Technosignatures during the VLA sky Survey: Survey Description and First Results

C.D. TREMBLAY,^{1,2} J.SOFAIR,^{3,4} L. STEFFES,^{5,2} T. MYBURGH,^{6,1} D. CZECH,² P.B. DEMOREST,⁴ R.A. DONNACHIE,^{6,1}
A. W. POLLAK,¹ M. RUZINDANA,² SIEMION, A.P.V.,^{1,7} S.S. VARGHESE,¹ AND S. Z. SHEIKH^{1,2}

¹SETI Institute, 339 Bernardo Ave, Suite 200, Mountain View, CA 94043, USA

²Berkeley SETI Research Center, University of California, Berkeley, CA 94720, USA

³Lafayette College, Department of Physics, Easton, PA 18045

⁴National Radio Astronomy Observatory, 1003 Lopezville Rd., Socorro, NM 87801, USA

⁵University of Wisconsin–Madison, Department of Astronomy, 475 N Charter St, Madison, WI 53703, USA

⁶Mydon Solutions (Pty) Ltd., 102 Silver Oaks, 23 Silverlea Road, Wynberg, Cape Town, South Africa, 7800

⁷Breakthrough Listen, University of Oxford, Department of Physics, Denys Wilkinson Building, Keble Road, Oxford, OX1 3RH, UK

ABSTRACT

Developing algorithms to search through data efficiently is a challenging part of searching for signs of technology beyond our solar system. We have built a digital signal processing system and computer cluster on the backend of the Karl G. Jansky Very Large Array (VLA) in New Mexico in order to search for signals throughout the Galaxy consistent with our understanding of artificial radio emissions. In our first paper, we described the system design and software pipelines. In this paper, we describe a postprocessing pipeline to identify persistent sources of interference, filter out false positives, and search for signals not immediately identifiable as anthropogenic radio frequency interference during the VLA Sky Survey. As of 01 September 2024, the Commensal Open-source Multi-mode Interferometric Cluster had observed more than 950,000 unique pointings. This paper presents the strategy we employ when commensally observing during the VLA Sky Survey and a postprocessing strategy for the data collected during the survey. To test this postprocessing pipeline, we searched toward 511 stars from the *Gaia* catalog with coherent beams. This represents about 30 minutes of observation during VLASS, where we typically observe about 2000 sources per hour in the coherent beamforming mode. We did not detect any unidentifiable signals, setting isotropic power limits ranging from 10^{11} to 10^{16} W.

Keywords: GPU computing (1969), Astrobiology (74), Search for extraterrestrial intelligence (2127)

1. INTRODUCTION

The place of humanity in the Universe and the existence of life is one of the most profound and widespread questions in astronomy and society in general. Throughout history, humans have marveled at the starry night sky. It is intriguing to consider the distances to the nearest stars, the origins of our Universe, and how life on Earth came into existence. During the past 60 yr, the active search for life on other planets has not resulted in any evidence that it has occurred (e.g. [Ma et al. 2023a](#); [Sheikh et al. 2021](#); [Smith et al. 2021](#)). Even the long-debated “Wow” signal ([Ehman 2008](#)) is no longer thought to be related to extraterrestrial life ([Méndez et al. 2024](#) and references therein). Therefore, we continue to wonder whether life is truly confined to this small planet orbiting an ordinary main-sequence star.

Starting in 2022, we built the Commensal Open-source Multi-mode Interferometric Cluster (COSMIC; [Hickish et al. 2019](#); [Tremblay et al. 2024](#)), offering the first Ethernet-based digital framework on the world-leading Karl G. Jansky Very Large Array (VLA) in New Mexico for rapid, real-time analysis of astronomy data. COSMIC was designed to provide an autonomous real-time pipeline for observing and processing data for one of the largest experiments in the search for extraterrestrial intelligence to date. To meet this design goal, we have constructed a digital signal processing system and computer cluster that takes a copy of each of the digitized antenna voltages, corrects the signals, calibrates the gains, coherently beamforms on targets of interest, forms an incoherent sum, and then searches for signals of a spectral and temporal nature consistent with our understanding of artificial technological signals (\sim Hz wide

emission signals; technosignatures). The output of this search is a database of “hits” and small cutouts of the phase-corrected voltage data for each antenna around the hits called “postage stamps.”

This is an opportune time for COSMIC to become operational, as it is possible to observe concurrently with the VLA Sky Survey (VLASS; Lacy et al. 2020). VLASS observes the entire northern hemisphere over two semesters in the VLA B-configuration, where Epoch 3 of the survey started in January 2023. Since March 2023, COSMIC has been operational and recording data from all 27 antennas with up to 1.2 GHz of bandwidth. The survey continued recording data from the second half of the sky starting in May 2024 to complete a full census at declination above -40 degrees. Observing along with this survey allows us to conduct one of the largest technosignature searches ever attempted within the frequency range of 2–4 GHz, covering almost a million of stars within two years.

The vast amount of data generated by the software pipelines running on COSMIC and other similar backends has led to the development of fast and efficient methods for locating narrowband and Doppler drifting signals. In Sheikh et al. (2019a), the authors discuss this problem in detail and conclude that the tree summation algorithm (also known as the Taylor tree method) is the most commonly implemented in modern technosignature searches due to its efficiency. However, the FastDD method (Houston 2023) offers some promising improvements. The main software program used by the community employing the tree summation method to date is TURBOSETI (Enriquez & Price 2019)¹, which is used on observations from the Robert C. Byrd Green Bank Telescope (e.g. Gajjar et al. 2021; Choza et al. 2024), Parkes 64m Telescope (e.g. Price et al. 2020; Sheikh et al. 2021), the Five-hundred-meter Aperture Spherical radio Telescope (e.g. Wang et al. 2023; Tao et al. 2023), and the Low-Frequency Array (Johnson et al. 2023).

Within the pipelines running on COSMIC, we use SETICORE², which is a GPU-accelerated implementation of TURBOSETI written in C++ with additional features: it includes postage-stamp extraction from the phase-corrected voltages of each antenna and visualization tools. This software is also implemented in the commensal technosignature search experiment on the MeerKAT telescope (Czech et al. in prep.). As with TURBOSETI, the user input parameters include the

signal-to-noise ratio (SNR) threshold and the Doppler acceleration drift rate³. It is possible to determine the precise expected drift rate based on the planet’s orbital motion (Li et al. 2022, 2023a), but this is only applicable to targeted surveys of known planetary systems. When detecting signals from nearby stars where planets are likely to exist but have not yet been discovered, as with COSMIC, broad search criteria are used. To search the data, we use an SNR threshold of 8 and a Doppler acceleration range of $\pm 50 \text{ Hz s}^{-1}$. This limit is much broader than necessary for known exoplanets (Sheikh et al. 2019a; Li et al. 2023b) but accounts for a broader range of possible scenarios where technology is orbiting off the planet but within the solar system (like Earth’s satellites). Coherently and incoherently beam-formed data are searched using these parameters, with a frequency resolution of 7.63 Hz per channel for the total 8-second recording segment, resulting in a drift rate bin size of 0.95 Hz s^{-1} . We also collect and save data with a drift rate of exactly 0 Hz s^{-1} . Such data are often discarded in many experiments as a way to limit the intrusion of terrestrial signals into the data. However, the 0.95 Hz s^{-1} may not provide the necessary resolution to detect signals arriving from systems similar to our nearest neighbors, such as TRAPPIST-1g (1.33 Hz s^{-1}) or Kepler-438 b (0.7090 Hz s^{-1}), as calculated by Li et al. (2022).

Once we have these detected signals and their associated metadata collected into a database, we need to devise plans to sort through these data to eliminate false positives likely associated with terrestrial radio emitters or instrumental artifacts and find new signals with astronomical origins. Although many of the experiments published so far involved manually investigating the dynamic spectra of the most promising events, this is no longer practical where the COSMIC pipeline identifies millions of signals per hour over thousands of sources. Although observational changes such as looking at signals that traverse across a multibeam receiver (i.e. Huang et al. 2023) or flagging known terrestrial signals within the real-time pipeline could be considered in the future, other ways of evaluating the data are required to investigate the data collected in the first six months of operation with COSMIC on the VLA.

In this paper, we describe a postprocessing strategy for the data collected and processed by COSMIC during VLASS observations. In Section 2, COSMIC’s observations during VLASS are summarized, and the ob-

¹ https://github.com/UCBerkeleySETI/turbo_seti; <https://ascl.net/1906.006>

² <https://github.com/lacker/seticore>

³ For a description of how the noise statistics are calculated and the software’s limitations see Choza et al. (2024)

servations that have been evaluated are described. In Section 3, we discuss the effects of a radio frequency interference (RFI) excision technique used after the data have been collected on COSMIC. In Sections 4 & 5 we discuss a postprocess for the evaluation of COSMIC-generated data for SETI and the first results from one of the VLASS observation nights. Finally, we discuss the impact of the results and conclusions of this work.

2. OBSERVATIONS

The observations described in this paper are based on data taken simultaneously with other VLA observing projects but analyzed separately, following the relevant National Radio Astronomy Observatory (NRAO) policies⁴ for commensal observation. Therefore, the COSMIC team does not control the observational strategy or calibration cadence. Our processing and analysis do not impact the standard NRAO operation and analysis used by the primary observer or the NRAO staff.

2.1. VLASS Observing Strategy

During VLASS, we observed and recorded data while the VLA was in the B-configuration and the hybrid configuration called B-North-A. Two observation campaigns, one in 2023 and one in 2024, represent the third epoch of this survey, which covers 80 percent of the sky. As part of this survey, large sections of the sky are rapidly covered by the telescope using the on-the-fly (OTF) mosaic method⁵. During this time, observations are broken into segments called “tiles”. Each tile covers between 25–40 deg² by moving in right ascension (RA) at a rate of 3.3 arc minutes per second, meaning there are approximately 5–10 seconds on each source before the source is outside the primary beam (the slew rate is slower at declination’s below ~ -20 degrees). After scanning in RA for approximately 10 minutes, the telescope moves in declination by 7.2 arc minutes and then scans again in RA covering the same distance as the previous track. Overall, it takes about 2 hours to observe each tile. For further details on the observation, see [Lacy et al. \(2020\)](#).

For COSMIC, we adopted an observing strategy where voltages are recorded in 8-second increments and processed separately. As described in [Tremblay et al. \(2024\)](#), the targets on which to form coherent beams, phase-centered pointing toward particular sources with a field diameter equal to the point-spread function, were

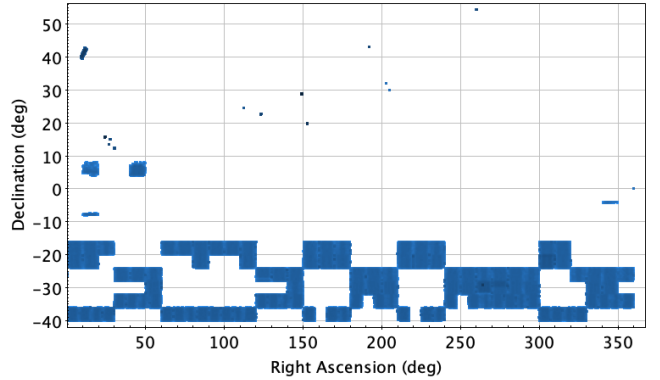


Figure 1. A plot of all the coordinates of targeted stars during VLASS recordings from 25 March 2023 to 15 June 2023. All recorded data of scientific quality that are contained with the COSMIC database for Epoch 3.1 are represented here.

selected based on the sources likely to spend the most amount of time within the half-power point of the telescope’s primary beam when a fully recorded field of view (FOV) is considered. The list of targets is from the technosignature target catalog, which itself is a selection of sources based on the *Gaia* Space Telescope DR2 catalog ([Czech et al. 2021](#)). For each two-hour observation of a single tile, the COSMIC software pipelines forms approximately 4000 coherent beams on sources in the target catalog.

During VLASS Epoch 3.1 in 2023, COSMIC observed and recorded science-ready data from 25 March 2023 to 15 June 2023, as shown in Figure 1. We accumulated 326,504 unique target fields (unique RA and Dec coordinates), representing 267,510 stars towards which we formed coherent beams, and 359,353,639 “hits” found by SETICORE. To assess the strategy and data quality we used 30 minutes of data observed on 15 April 2023 during the recording of a partial VLASS tile. The VLA was in B-configuration and recording data at 2–4 GHz in the 8-bit recording mode, and 24 of the 27 antennas were online and recording for the duration of the observation. Every 15 minutes, the VLA conducted phase calibration scans, with at least one scan of 3C 286 per tile used for flux calibration.

2.2. COSMIC Recording and Processing Setup

COSMIC is divided into four distinct segments (digital signal processing, calibration, beamforming, and search), the last three of which take place in real time and are outlined in Figure 2 and described in detail in [Tremblay et al. \(2024\)](#). Digital signals are received and processed by the first rack of COSMIC. Each field programmable gate array (FPGA) board receives the digital signals from two of the antenna’s digital transmis-

⁴ <https://science.nrao.edu/observing/proposal-types/commensal-observing-with-nrao-telescopes>

⁵ <https://science.nrao.edu/facilities/vla/docs/manuals/obsguide/modes/mosaicking>

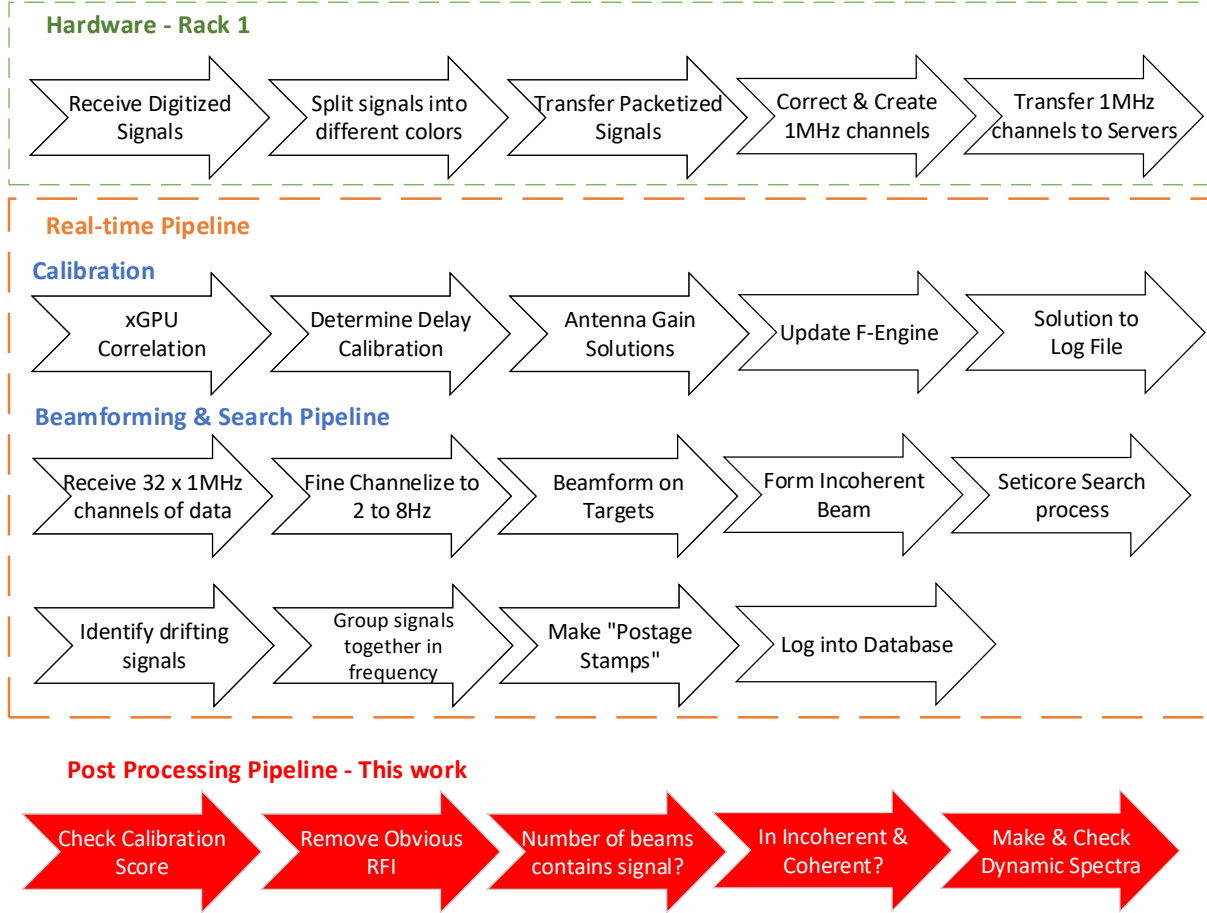


Figure 2. Summary of the pipeline implemented in COSMIC. Based on the telescope’s observational intent, the data will either flow from the hardware to the calibration pipeline or from the hardware to the search pipeline on the GPUs. The postprocessing step, which will be described later in this work, is a separate data flow and does not happen in real time. A more detailed depiction of the process can be found in Figures 3 and 8 of Tremblay et al. (2024)

sion streams using existing VLA firmware provided by NRAO (but processes each independently). They also

- compensate for delays due to both signal propagation from the astronomical source of interest to the VLA antennas and fiber optic signal propagation from the antennas to the COSMIC system;
- removes local oscillator offsets and creates coarsely channelized 1 MHz channels from the broadband input;
- form packets of digitized coarse channels to transmit via a 100 Gb Ethernet switch to a runtime-determined downstream processing node (the GPU node).

Incoming data from the VLA consist of two intermediate frequencies (IFs) of 1024 MHz each, for a total of 2048 MHz, when in the 8 bit recording mode. During the 2023 VLASS observations, we had up to 15 operational GPU servers (some shut down as we worked on system stability), each containing two processing nodes. In order to search for signals within the 960 MHz of bandwidth, we used the 100 Gb switch to transfer 32×1 MHz coarse channels to each node, which were then split between the two IFs (480 MHz each) between the 2 and 4 GHz that the COSMIC system ingested. As shown in Figure 3, there was significant RFI on the edges of the band, so we focused the processing and search on 2.5–3.5 GHz, as will be further discussed in Section 3.

Each 32 MHz of bandwidth is processed through either the calibration pipeline or the technosignature search

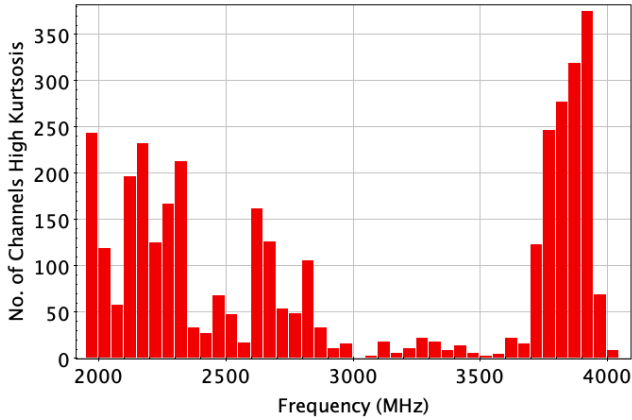


Figure 3. Histogram showing the number of frequencies per frequency window that have high kurtosis, implying high levels of RFI. The edges at 2–2.5 GHz and 3–3.5 GHz show significant RFI. Therefore, for VLASS, the central frequency range of 2.5–3.5 GHz was processed and searched.

pipeline. The VLA observations are set with a series of “intents,”⁶ which are assigned by the person creating the scheduling block. When the intent contains the word “calibration” the data are processed through the calibration pipeline, as defined in the second line of Figure 2. When the intent is “OBSERVE TARGET,” the data are run through the technosignature search pipeline. The following sections describe these processes in detail. The information about what the pipeline detected is recorded to an SQL database, and “postage stamps” of the calibrated voltages are saved on disk.

The data from the 15 April 2023 observations include coherent beamformed results on 511 unique *Gaia* DR2 sources from the catalog created by Czech et al. (2021), some of which were searched for drifting signals multiple times when the declination strips overlapped with a previous slew of the telescope. We also searched within the incoherent sum in each 8 seconds of data.

2.3. Calibration

The COSMIC processing pipeline follows standard calibration procedures for radio astronomy data with a strong focus on delay and phase calibration. Currently, the automated pipeline does not conduct absolute flux density calibration. However, the data are saved on disk, and this can be applied to the data prior to reporting any values. The pipeline uses the xGPU⁷ (Clark et al. 2013) software correlator to cross-correlate the raw voltages and create the visibility data products in four polariza-

tions (RR, LL, RL, and LR, where R and L refer to right and left circular polarization, respectively), which are saved in *uvh5* files⁸ on the storage nodes. Once each of the 32 MHz of data is correlated and the delays and gain solutions are computed, the data are collated back together across all frequencies on the COSMIC head (computer) node to be reorganized and reported. The new residual delay and phase solutions are uploaded to the FPGAs, and the resultant solutions are saved in a *json* file format in a folder with the *uvh5* file for posterity.

As part of the calibration process, after the solutions are brought together and sorted by frequency, the solution quality is graded based on the stability of the phases. With each new calibration processing pipeline application, the FPGA signal corrections get updated. Therefore, each new calibration has had some calibration applied, and the results of the phase are really a difference from the previous calibration. The main grading criterion we use to define a good calibration compared to a bad calibration is phase stability. When the phases are flat across frequencies (per each polarization and antenna), the resultant grade is given the value of 1. When the phases are chaotic, uncorrelated, or contain significant wraps, the grade value decreases toward 0. See Equation 9 in Tremblay et al. (2024) for details on how the overall grade is computed in detail.

Uncorrelated individual frequency channels or antennas, often caused by an incorrect delay model or the antenna still slewing during recording, can corrupt the overall grade value. That is why, in addition to the overall grade, we compute a grade per frequency channel across antennas (Equation (8) in Tremblay et al. (2024)) and a grade per antenna across all frequency channels (Equation (7) in Tremblay et al. (2024)) to better isolate these instances. However, these grades are determined before the calibration is applied and representative of a differentiation between calibration runs more than an accurate measure of the determined calibration values for the current observation.⁹

Examples of the calibration phases plotted as phase degrees versus frequency are shown in Figure 4. The overall calibration grade and the plots, along with other diagnostic plots, are sent to a SLACK¹⁰ channel for posterity and to allow those reviewing the data for scien-

⁶ <https://www.aoc.nrao.edu/~cwalker/sched/INTENTS.html>

⁷ <https://github.com/GPU-correlators/xGPU/blob/master/README>

⁸ https://pyuvdata.readthedocs.io/en/v1.5/_modules/pyuvdata/uvh5.html

⁹ Current automated processes on COSMIC generate a predictive overall grade from the calibration gain solution that is used to predict phase stability in subsequent target observations. However, this was not implemented at the time the data evaluated in this paper were written.

¹⁰ <https://slack.com/intl/en-gb/>

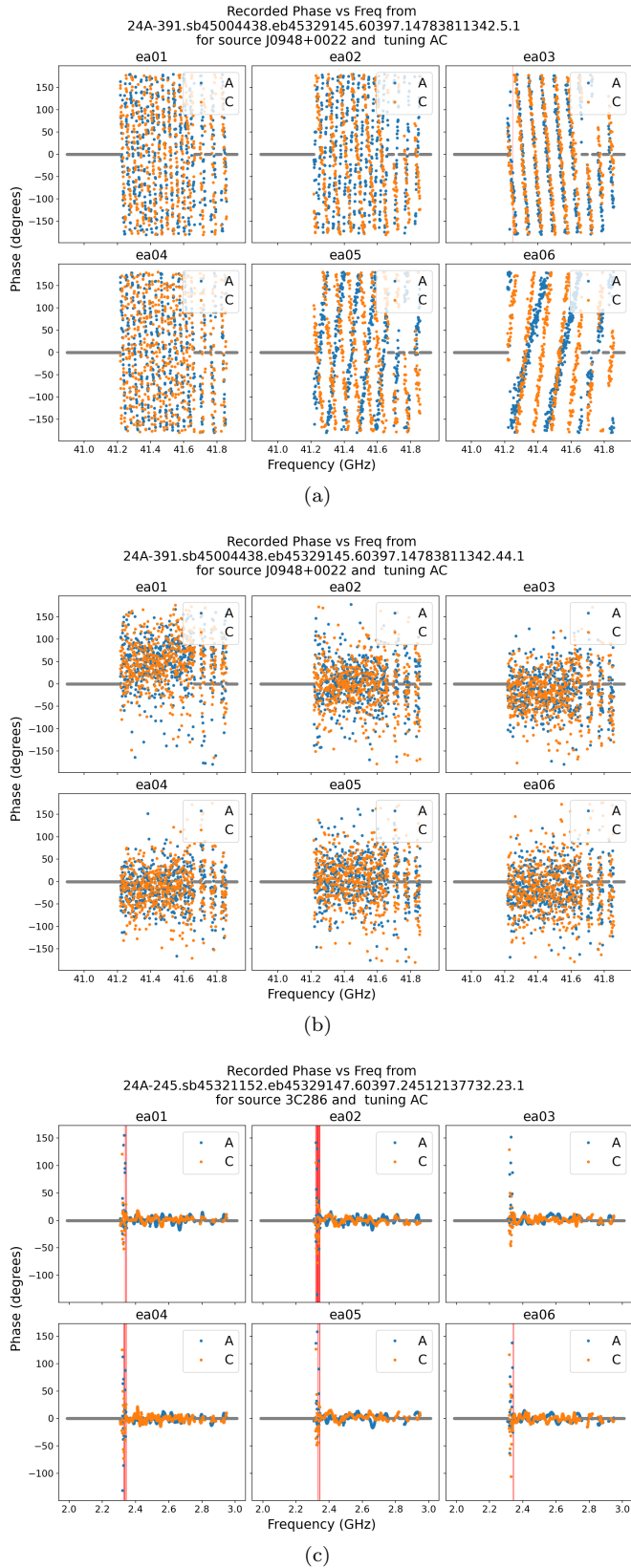


Figure 4. Example calibration plots from the AC tuning generated by plotting the phases prior to the calibration being applied. In (a), the overall grade is <0.2 , (b) has a score of 0.639, and (c) has a score of 0.991. A score greater than 0.6 is considered a “good” calibration, as this represents a score prior to the correction to the FPGA. Therefore, it shows the ease with which a solution can be found more than the actual solution. The red vertical strips indicate 1 MHz channels that are flagged as containing RFI signals during the calibration run.

tific use a rapid review and evaluation of the calibration quality during the observations of interest. When a calibration grade is above a value of 0.6, representing that there is no more than a 40% drop in sensitivity, and chosen as value suggestive that all but one or two antennas have phases that are easy to calibrate, no further investigation of the solutions is completed. The resultant science data proceeding the calibration are taken as worthy of investigation. When the score is less than 0.6, the plots and other diagnostics are reviewed to see if the data are scientifically valid. These phase solutions are critical; in coherent beamforming, improper phase solutions will cause the coherent beam to be offset from the position of the target source, creating either a significant reduction in sensitivity or a smeared point-spread function (depending on the severity of the problem).

In the last year, we improved the phase solution calculation by flagging for 1 MHz channels subject to narrow-band RFI. For the spectrum of a given tuning, baseline, and polarization averaged over time, a channel that satisfies

$$|f_i - \text{median}(f)| \geq 5 \times |\text{MAD}(f)| \quad (1)$$

is considered to contain RFI, where f is the frequency, i the channel index, and MAD the *median absolute deviation*. A flagged spectral value f_i is replaced with the $\text{median}(f)$ so as not corrupt the calculated gains and, in turn, the applied phase solution. We note that while I RFI emission is largely coherent, it is not usually continuous, and so deriving gains from RFI-contaminated signals will likely lead to gain solutions for that channel that do not accurately represent the scientific data in the target observation.

For longevity and retrospective analysis, two calibration tables in the COSMIC database are created. They are ‘AntennaCalibration’ and ‘ObservationCalibration.’ In the ‘ObservationCalibration’ table, we store the overall calibration details linked to the calibration observation. This is mostly used for grade performance evaluation in time studies. ‘ObservationCalibration’ stores the calibration observation ID, the reference antenna, the overall grade, and the output directory for the calibration observation and its products. ‘AntennaCalibration’ stores the antenna and tuning-specific calibration details, which are used to further inspect irregularities noted in grade evaluation studies. For each antenna entry, while linked to the calibration observation ID, we store the antenna name, tuning, number of coarse channels processed in the calibration run, and number of RFI-flagged channels during the calibration run.

To evaluate the stability of the calibration score and COSMIC’s pipeline operation, we plotted the data

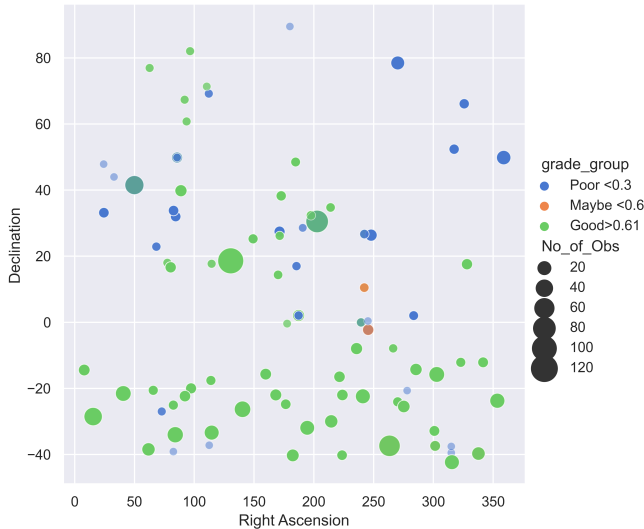


Figure 5. Calibration results for 2 months of operation. The colors of the bubbles represent the grade of the calibration, where the higher value is a lower SNR across the phase and the size of the bubble represents the number of times the source was observed. As can be seen, the calibration is good most of the time.

from May and June 2023. The most common calibrators used by observers and recorded by COSMIC were J2355+4950, J1024-0052, J1033+6051, and 3C286. As demonstrated in the plot in Figure 5, more than 80% of the calibrations across a range of frequencies have a score of greater than 0.6. In particular, the best scores are often from strong phase and flux calibrators used frequently in the calibration of VLA data. Many of the poor-quality data plots (in blue) are often from weak phase calibrators chosen by the observer or due to a frequency change with respect to previous observations.

For the observations reviewed here from 15 April 2023, the grade of the observations varied significantly but most were in the range of 0.4–0.9. All corrected gain plots show good phase stability for at least 24 antennas.

2.4. Beamforming during OTF Scans

Although the beamforming code and science verification are discussed in depth in Tremblay et al. (2024), here we discuss their application when the telescope is using the OTF scanning mode as used during VLASS. The COSMIC pipeline uses the beamforming code “Breakthrough Listen Accelerated DSP Engine” (BLADE¹¹), which was developed as part of the refurbishment of the Allen Telescope Array in California, USA.

The data recorded during an OTF scan are partitioned into files spanning 8.338608s each. The OTF observation system ensures a constant phase across each file by instructing the antenna to only update phase centers on file boundaries. This limit is also determined as the upper limit after which beamforming and dedoppler search cannot be achieved within “real time.” The coordinates of the beams formed are sourced from candidates within the half-power point of the FOV around the phase center as received from the target selector system (see Figure 16 in Tremblay et al. 2024). Consequently, the beam coordinates are independently derived from each 8s partition of the data. Before the actual beamforming computation, each coarse channel is upchannelized to the requested resolution without reducing the number of fine spectra below 50 (typically 64 time steps for VLASS observations with an FFT size of 131,072), to the benefit of the dedoppler search, and while keeping the overall processing time within “real-time” bounds. The upchannelization exhausts all time samples for the coarse channel before iterating to the subsequent coarse channel. The following beamforming computation processes each fine spectrum. We collect the whole time span before we do a dedoppler search. Therefore, the dedoppler search is computed iteratively across each upchannelized, beamformed coarse channel, repeating for each time partition of the OTF scan.

To ensure the beamformer coefficients are updated appropriately, an observation of the methanol maser emission at the star-forming region W51 (e.g. Etoke et al. 2012) was taken on 31 May 2023 using the same OTF parameters as VLASS and 3C286 was used to calibrate the data through the standard pipeline. By plotting the time samples as a function of normalized beam power for the frequency channel that contains the peak emission of the maser, we see a pattern that mimics the primary beam response of the VLA dishes as expected, shown in Figure 6¹² (Perley 2016).

2.5. Real-time Search Pipeline

Each 8s segment of recorded data is searched for narrowband signals following beamforming. For this, we use the software package SETICORE, which uses the same Taylor tree method as TURBOSETI but is rewritten for GPU acceleration. In the pipeline running COSMIC during VLASS, SETICORE searches for narrowband signals that have an SNR above ten and across a drift rate of $\pm 50 \text{ Hz s}^{-1}$. For each signal it detects, the metadata about the signal characteristics are logged into an SQL

¹¹ <https://github.com/luigifcruz/blade>

¹² This observation was taken during test time with 21 antennas online.

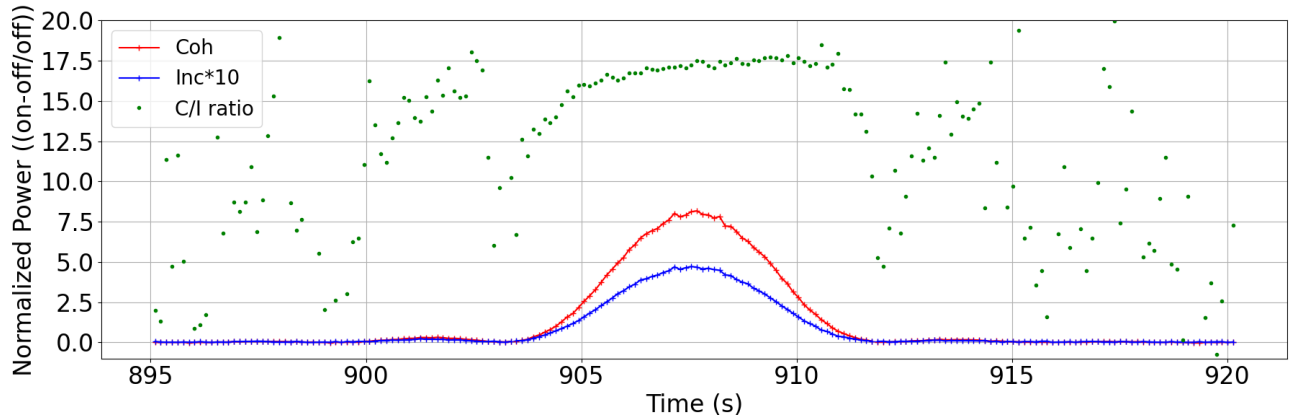


Figure 6. The plot above shows the power over time for the frequency channel containing the peak intensity of the W51 6.7 GHz methanol maser emission. The shape of the line is expected to correspond to the antenna’s primary beam response. As a comparison, the power response of coherent and incoherent beams (multiplied by a factor of 10 to improve visibility) is plotted, along with their ratio. The ratio is ideally expected to equal the number of antennas used in the summation, which was 21 in this test. Imperfect calibration reduces the ratio away from the ideal value. The high scatter of the ratios away from the peak is due to large errors from small, noisy values.

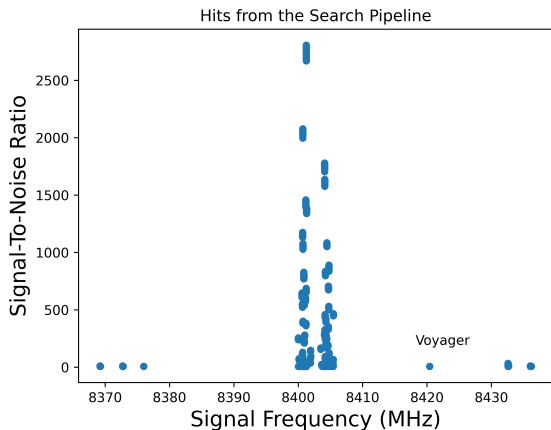


Figure 7. A plot of the signal-to-noise ratio versus observing frequency showing all of the hits found in the observations toward Voyager detected by SETICORE.

database, and a segment of the calibrated and channelized voltages is saved as “postage stamps.”

To test the efficiency of the real-time pipeline at detecting technosignatures, we pointed the telescope toward the Voyager I space satellite using VLASS-style observations. We then let the real-time pipeline run with no input except to prioritize a coherent beam toward Voyager’s location. As shown in Figure 7, SETICORE recorded information on 4121 signals. Voyager’s signal around 8420 MHz was one of these signals detected. We note that additional testing will be discussed in a future publication with the full VLASS data release.

3. RADIO FREQUENCY INTERFERENCE

As mentioned in Section 1, the COSMIC postprocessing pipeline searches for signals that are similar to anthropogenic sources of radio emissions in their spectral and temporal signatures. Despite providing a valuable reference for the characteristics of technosignatures, human-made radio emissions are also one of radio astronomy’s greatest hindrances. Given the ubiquity of anthropogenic radio emission technology (e.g., cellular networks, satellite radio, etc.), any radio telescope located near enough to humans will detect these unwanted radio signals. For COSMIC, this means signals that do not originate from the target source will be picked up and flagged as potential technosignatures. The signals that cause these false positives are known as RFI. We therefore have created a software package described below to identify prominent and persistent sources of RFI during calibrator observations. The assumption here is that the signals detected in a short observation toward the calibrator are all from sources of terrestrial radio emission and not signals of interest.

3.1. Classification and Identification

Two characteristics of the technosignatures we are seeking are that they could be narrowband (signal contained in \sim Hz wide channels) and that their frequency would change over time as a result of the Doppler effect (Sheikh et al. 2019b; Li et al. 2022). Technosignatures can be distinguished from typical astronomical sources by their widths in frequency space. The finest-frequency astronomical emitters discovered thus far are found to produce signal widths on the order of 10^2 Hz (Gray 1999; Zhang et al. 2020).

RFI permeates astronomical data, causing narrow-band spikes in detected power with time-varying intensities and frequency instabilities^{13,14}. The similarities between terrestrial radio signals and technosignatures make it challenging to determine if the source of a signal is of extraterrestrial origin or not. Contemporary technosignature search algorithms therefore output a large number of false positives. Thus, the search for an extraterrestrial needle in a “cosmic haystack” (Wolfe et al. 1981; Wright et al. 2018) becomes exponentially more challenging in the presence of RFI. Even if a signal can be confirmed to be anthropogenic, its highly variable properties make it troublesome to remove.

Currently, technosignature searches employ a variety of RFI removal techniques, including observational strategies and postobservation data analysis. Observational techniques include the use of cadenced-based observation (some time pointing away from the primary source) for single-dish telescopes (e.g. Price et al. 2020), and the analysis of which beams—coherent and/or incoherent—a signal is found in for interferometers (demonstrated in this work). However, multitelescope follow-up is also a viable and suggested method for signal confirmation (i.e. Ma et al. 2023a; Johnson et al. 2023). The identification of terrestrial radio signals includes the analysis of χ^2 statistics (Weber et al. 1997), the use of machine learning (Zhang et al. 2020; Ma et al. 2023b), RFI subtraction using a reference signal (Briggs et al. 2000), and much more. Many of the techniques that fit into the latter category are mathematically intense and/or computationally expensive. Here we seek to develop a new method to swiftly flag frequency ranges that are heavily tainted by RFI to allow for more efficient data analysis.

3.2. RFI Identification with Excess Kurtosis

Our first line of defense against RFI uses the statistical measure of excess kurtosis, *exkurt*, which gives the measure of the infrequent outliers in a distribution. We use the Fisher¹⁵ definition of kurtosis, *kurt*, in this work, given by

$$exkurt = \frac{\mu_4}{\mu_2^2} - 3, \quad (2)$$

where μ_4 is the 4th central moment of the distribution and μ_2 is the 2nd central moment (variance). Under this

definition, a standard normal distribution has an excess kurtosis of 0.

The astronomical noise in our data is expected to have power normally distributed in any given frequency bin due to the incoherence of the electromagnetic waves collected by the VLA (Smith et al. 2022). Therefore, large enough deviations from Gaussianity imply the presence of a signal. We can use this to our advantage to rapidly flag frequency bins that are dominated by RFI, or “dirty.” To filter out the false positives in the database during data postprocessing, we developed a new PYTHON package called the Categorization of RFI in COSMIC with Kurtosis for Extraterrestrial Searches (CRICKETS¹⁶).

The use of excess kurtosis to flag RFI-dominated frequencies is not a novel technique. Nita & Gary (2010) proposed the spectral kurtosis estimator, \widehat{SK} , a mathematical object used to flag RFI within the context of radio astronomy. This estimator was generalized by Nita et al. (2019) and implemented in HYPERSETI¹⁷, a PYTHON package designed to search spectral data for technosignatures in both single-dish and interferometric data. COSMIC currently runs a different technosignature search package (SETICORE) that does not have a robust RFI flagging method. The lack of this key function in the COSMIC beamforming and search real-time pipeline is the primary motivation behind the use of CRICKETS within the pipelines running on COSMIC.

3.3. CRICKETS Application

Frequency, power, and time data are fed to CRICKETS in the form of a *filterbank* file generated from forming an incoherent beam on a VLA observation toward a calibrator source. This was done with the assumption that no technosignatures would be in the field surrounding the calibrator and that the emission detected in the data would be dominated by broadband emission from the bright calibrator source and RFI. CRICKETS reads these *filterbank* files in using the BLIMPY¹⁸ PYTHON package. Once the file is loaded in, the power is averaged over the time axis and tabulated with their respective frequencies.

The next operations that CRICKETS performs are to organize the data to a user-specified number of frequency bins, rescale the data¹⁹ by a factor of 10^9 , and

¹³ <https://science.nrao.edu/facilities/vla/docs/manuals/obsguide/rfi>

¹⁴ https://www.parkes.atnf.csiro.au/observing/rfi/how_does_rfi/how_does_rfi.html

¹⁵ <https://docs.scipy.org/doc/scipy/reference/generated/scipy.stats.kurtosis.html>

¹⁶ <https://github.com/jareds-laf/CRICKETS>

¹⁷ <https://github.com/UCBerkeleySETI/hyperseti>

¹⁸ <https://github.com/UCBerkeleySETI/blimpyp>

¹⁹ The data is re-scaled to avoid any infinities in the excess kurtosis calculations.

to calculate the excess kurtosis (Equation 1) of every frequency bin using SCIPY. The excess kurtosis calculation is computed using all of the fine-frequency channels within a given bin. Bins that are dominated by RFI are flagged based on their excess kurtosis relative to the excess kurtosis threshold, which is the second user-specifiable quantity in the analysis. Bins can have an excess kurtosis of a certain magnitude before being flagged as dirty if they exceed the threshold. Bins flagged as dirty are compiled and output to a *CSV* file using PANDAS.

3.4. S-band RFI Determination and Results

We used CRICKETS to analyze 48×32 MHz subbands covering the S-band (2–4 GHz) non-continuously. We generated an incoherent sum using BLADE²⁰ version 0.7.4 toward the source 3C286 (RA: 4h9m22s, Dec: 12d17m39.8475s) on May 10th, 2023 with the VLA in the B-configuration. We analyzed the data observed during Epoch 3.1 of VLASS using the tool CRICKETS to determine the number of frequency bins and excess kurtosis threshold that could be applied to the entire sample of data.²¹ Generating the time-averaged power spectra and excess kurtosis plots revealed that 256 bins per file (corresponding to 125 kHz per bin or 15,625 fine channels per bin) with an excess kurtosis threshold of 5 was optimal. In some files, regions dominated by RFI went unflagged, but if the threshold was lowered even slightly, regions in other files without RFI would have been falsely flagged. With the parameters we chose, about 29.88% of the frequencies evaluated were flagged as dirty (see Figure 8).

Figure 9 serves as an example of how CRICKETS performed on one of the 32 MHz subbands. It excelled at marking strong, isolated RFI signals and regions of denser RFI. One of CRICKETS most consistent problems was failing to identify or falsely identifying RFI in the frequency ranges where the sinc-like function of the polyphase filterbank (PFB) response for each 1 MHz coarse channel approached a local minimum. To greatly improve the reliability of CRICKETS, we are in the process of adding a PFB response subtraction function. A full analysis and plots from each subband are found in the Undergraduate (NSF REU) program student report²².

²⁰ <https://github.com/luigifcruz/blade>

²¹ In the future, regular scans will be done to look for the persistent nature of RFI and find sources that change as a function of time and elevation.

²² <https://www.nrao.edu/students/2023/Reports/SofairJared.pdf>

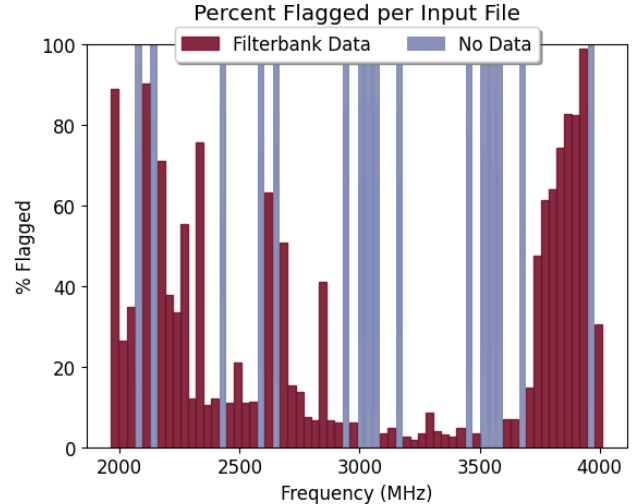


Figure 8. Percentage of frequencies flagged per filterbank file. Each dark red rectangle represents a filterbank file. Each dark blue rectangle represents a frequency range within the S-band for which we did not have data.

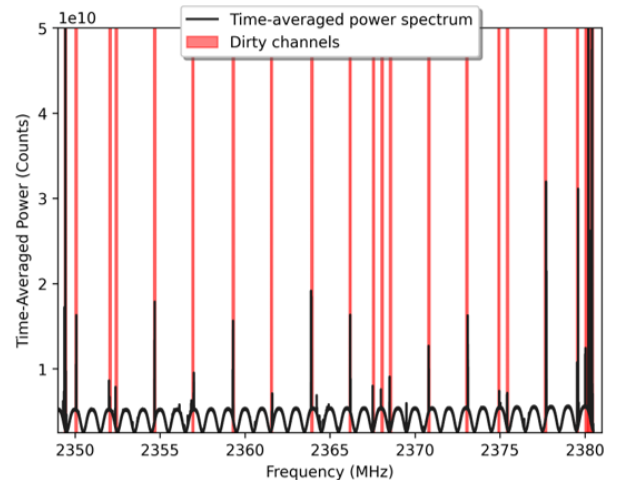


Figure 9. Example of a time-averaged power spectrum in the 2348.5–2380.5 MHz band. The transparent red regions mark the locations where CRICKETS detected RFI. The fine-frequency spikes in time-averaged power are a result of RFI. We know this to be true because these data come from observations of the calibration source 3C286. The sinc-like pattern at the bottom of the plot is a result of the polyphase filterbank (PFB) process, which is a necessary step in COSMIC’s signal processing procedures. This will be discussed further in Section 3.4.

From the CRICKETS pipeline, a *CSV* file and a PYTHON NUMPY array were created listing all channels that had excess kurtosis. This information was stored on the COSMIC computers to be applied in the post-processing steps when evaluating the data collected during VLASS as a first-level removal of significant false pos-

itives. We note that not all of the subbands recorded during VLASS by COSMIC were evaluated by CRICKETS due to some data being lost resulting from a storage disk failure. However, in the future, we will work to make this a more robust process, as described in Section 6.

Based on this analysis and plots provided by NRAO for the VLA RFI environment, COSMIC recorded the band between 2.5 and 3.5 GHz for our observations during VLASS. Therefore, avoid the regions of the spectrum that contain the strongest RFI.

4. THE ARTISTIC POSTPROCESSING PIPELINE

After passing the data through SETICORE, potentially millions of hits are identified across the range of frequencies searched, far too many hits to identify likely technosignature candidates individually with visual inspection. To solve this problem, we developed the Anomaly, RFI, and Technosignature Identification Search and Tabularization In COSMIC (ARTISTIC) postprocessing pipeline. In this pipeline, extraterrestrial technosignatures are characterized by a set of assumptions and conditions that, if not met, are used to eliminate hits that do not meet these assumptions. The details of these assumptions are explained below and summarized in Figure 11. For the data from 15 April 2023, over 29,000 hits were identified by SETICORE and distributed across the 2.5–3.5 GHz frequency band as shown in Figure 10, with the majority of false positives associated with RFI.

Initially, the pipeline evaluates the calibration solutions for the set of observations being evaluated. We first verified the calibration grade score and then reviewed the plots to ensure that the data quality was of scientific merit, as discussed in Section 2.2. If the phase calibration was poor, this would result in coherent beams not being formed at the sources of interest and reduce the overall power of the detected signal.

Second, the data are evaluated against the textscCRICKETS output described in Section 3.4 and a user-selected SNR threshold (a changeable value determined to best remove additional significant sources of time-variable RFI and spurious antenna artifacts). A description of how the software determines the noise level and the limitations of this method are discussed in detail in Choza et al. (2024).

As a result of using an interferometer for SETI and forming multiple coherent beams, we can filter the results based on this target strategy. There is no localization of a source of emission if it is detected in all coherent and incoherent beams. As a result, these signals are immediately removed from the list of candidate signals. If

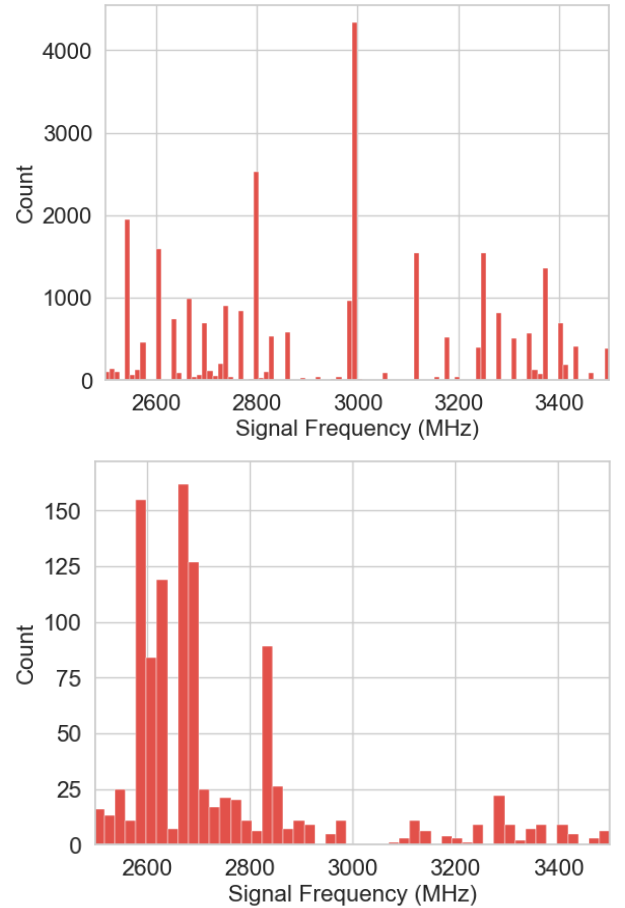


Figure 10. Top: distribution of detected signals by the real-time pipeline before any filtering for RFI. Bottom: number of channels flagged with high kurtosis per frequency bin. When the two plots are compared, there are frequency ranges where there are not many flagged channels but a large number of hits.

a hit at a given frequency is only detected within a single coherent beam, we can assume the signal is localized in the sky and thus becomes a potential signal of interest. If the emission is found in multiple beams, then other criteria are considered, such as the ratio of the signal strength in the coherent and incoherent beams and how close the coherent beams are formed. We assume that a signal emitted by a single source should be relatively localized to within the single coherent beam, except when a strong source is present and therefore could have a signal that bleeds into an adjoining beam. As described in Section 3.7.2 in Tremblay et al. (2024), the ratio of the normalized power from the coherent and incoherent beams should be equal to the number of antennas used in the observation.

The final stage of each track within the ARTISTIC pipeline is to determine if a signal is likely RFI or if it is worth investigating by creating dynamic spectra. At

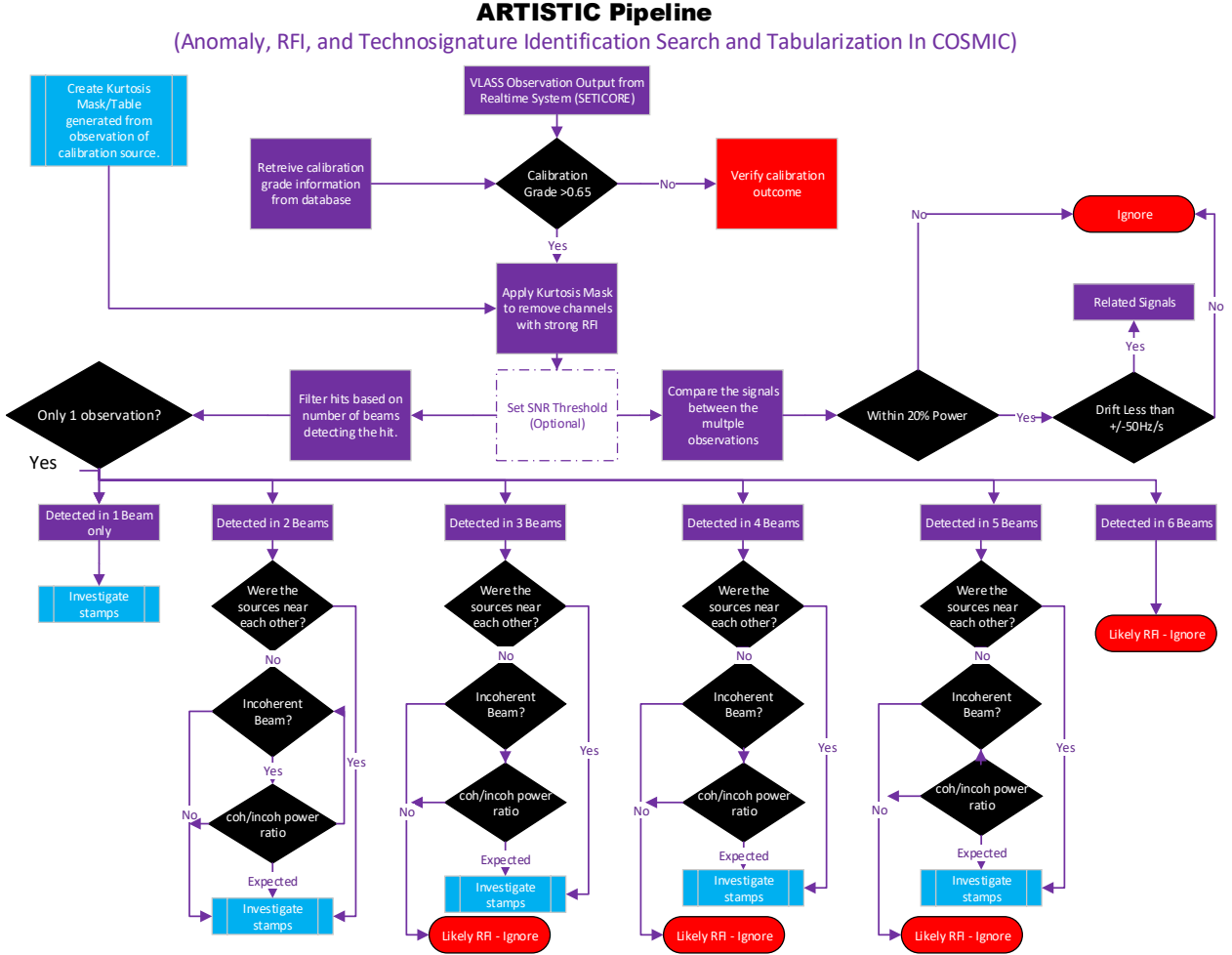


Figure 11. A flow diagram showing the logic behind the ARTISTIC pipeline that can be applied to any set of observations.

the end of the real-time processing pipeline, a series of files containing segments of raw voltages from each on-line antenna is saved. We can use these, combined with the visualization tools within SETICORE and the information about the beam coordinates stored in a beamformer *bfr5* file, to recreate the coherent and incoherent beams and therefore the dynamic spectra. All signals that were only detected in a single antenna or a small group of antennas were also immediately discounted as being of astronomical origin. This is done by calculating the SNR at the signal position for each antenna, using the SETICORE viewer software.

Due to the OTF scan strategy, there is an overlap in the sky; therefore some sources are observed multiple times within the same VLA scheduling block. We can use this second observation within a short period of time to apply additional filters, as per Figure 11. Any signal of interest that has a time separation of ~ 10 minutes should be drifted in frequency due to Doppler accelera-

tion but localized to the same position in the sky. We searched for signals that were sky localized and drifted no more than $\pm 50 \text{ Hz s}^{-1}$.

5. RESULTS

To evaluate the effectiveness of the ARTISTIC pipeline, we use data from 25 April 2023. This represents a 2-hour observation run with COSMIC, covering 468 beamformed sources and a total of 511 coordinates (when adding in the incoherent beam phase center). We found all plots and results from calibration on 15 April 2023 were consistent with high-quality data after the F-engine correction.

The data were compared to the outputs by CRICKETS to look for signals that passed or were contained within the flagged RFI regions. We also use an SNR threshold of 100 to remove signals impacted by intense instrumental artifacts that appear in a single or only a pair of antennas. Upon quality checks of the raw volt-

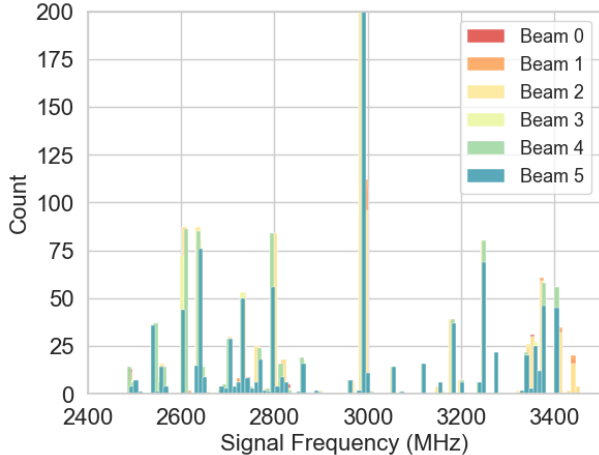


Figure 12. A histogram demonstrating the signals detected for each frequency per each beam. This shows that many of the signals are in similar frequency ranges and at a similar number of detected signals per frequency.

ages, it was determined that this value removed most artifacts found only a few of the antennas and not suggestive of signals with astronomical origins. With these two filters, we reduced the 29,390 signals down 77% to 9,708 signals of potential interest.

As shown in Figure 12, the majority of the signals detected at each frequency are in all of the beams. After the first two stages, we have

- 1646 in Beam 0;
- 1650 in Beam 1;
- 1657 in Beam 2;
- 1615 in Beam 3;
- 1625 in Beam 4;
- 1515 in Beam 5 (incoherent beam);

When filtered, no signals were contained in only a single (coherent or incoherent) beam. An example of one of the signals detected by COSMIC is shown in Figure 13, where the signal is seen in multiple coherent beams and the incoherent beam.

To determine how bright a signal would need to be for each source in order for us to detect it, we compute the minimum equivalent isotropic power ($EIRP_{\min}$) for the 511 sources,

$$EIRP_{\min} = 4\pi d^2 F_{\min} \quad (3)$$

where the relationship to the detectable power is based on a distance squared. The F_{\min} value is determined by dividing the minimum flux density the bandwidth of the

transmitting signal. For this experiment, we use a minimum flux density of 13.92 Jy which is the 8σ value of the flux density limit from the VLA sensitivity calculator. The bandwidth is set as equal to the channel width of ~ 8 Hz.

As shown in Figure 14, the $EIRP_{\min}$ values range from 2.32×10^{11} to 2.09×10^{16} W. Based on the distances calculated using parallax in Czech et al. (2021), the sources range in distance between 4.3 and 1296 pc. By using the value for the Arecibo radio telescope transmitter power (L_A) of 2×10^{13} W from Siemion et al. (2013), we can calculate the ratio ($EIRP_{\min} \div L_A$) of this value for each source in our survey. As a result, we established a value range between 0.012 and 1045, which suggests that if an Arecibo transmitter was located on a planet orbiting the nearest star 4.3 pc away, we would be able to detect it at least at an 8σ level.

6. DISCUSSION

The field of astronomy is experiencing a relatively new problem called "big data." The idea is that we are receiving increasing quantities of data that must be sorted in new ways in order to find information of scientific interest. Although using the world's population and their excitement to filter out signals of interest through their collective enthusiasm is a feasible method for certain kinds of projects (Li & Margot 2024), we could quickly overload people if we did this with all of the data generated by COSMIC. Therefore, creating postprocessing pipelines through a series of logical steps that can be followed by humans or through machine learning/neural networks is necessary as we progress with our data collection.

As shown in Figure 15, within the last 11 months of operation, COSMIC has observed over 950,000 fields and is rapidly becoming one of the largest SETI experiments ever designed. If any signal is identified by the postprocessing pipeline described in this paper or another, we have successful proposals with the VLA, the Very Long Baseline Array, the Allen Telescope Array, and the Parkes 64m Telescope to follow up on those signals within a 1-week time frame. However, we note that at this time, the time frame for detecting signals for follow-up will take months until postprocessing becomes more automated. However, this post detection protocol will allow us to identify any potential signals of interest by using different signal pathways, telescopes, and locations. This network is critical to understanding the nature of any signal detected that cannot immediately be dismissed as RFI.

7. CONCLUSION

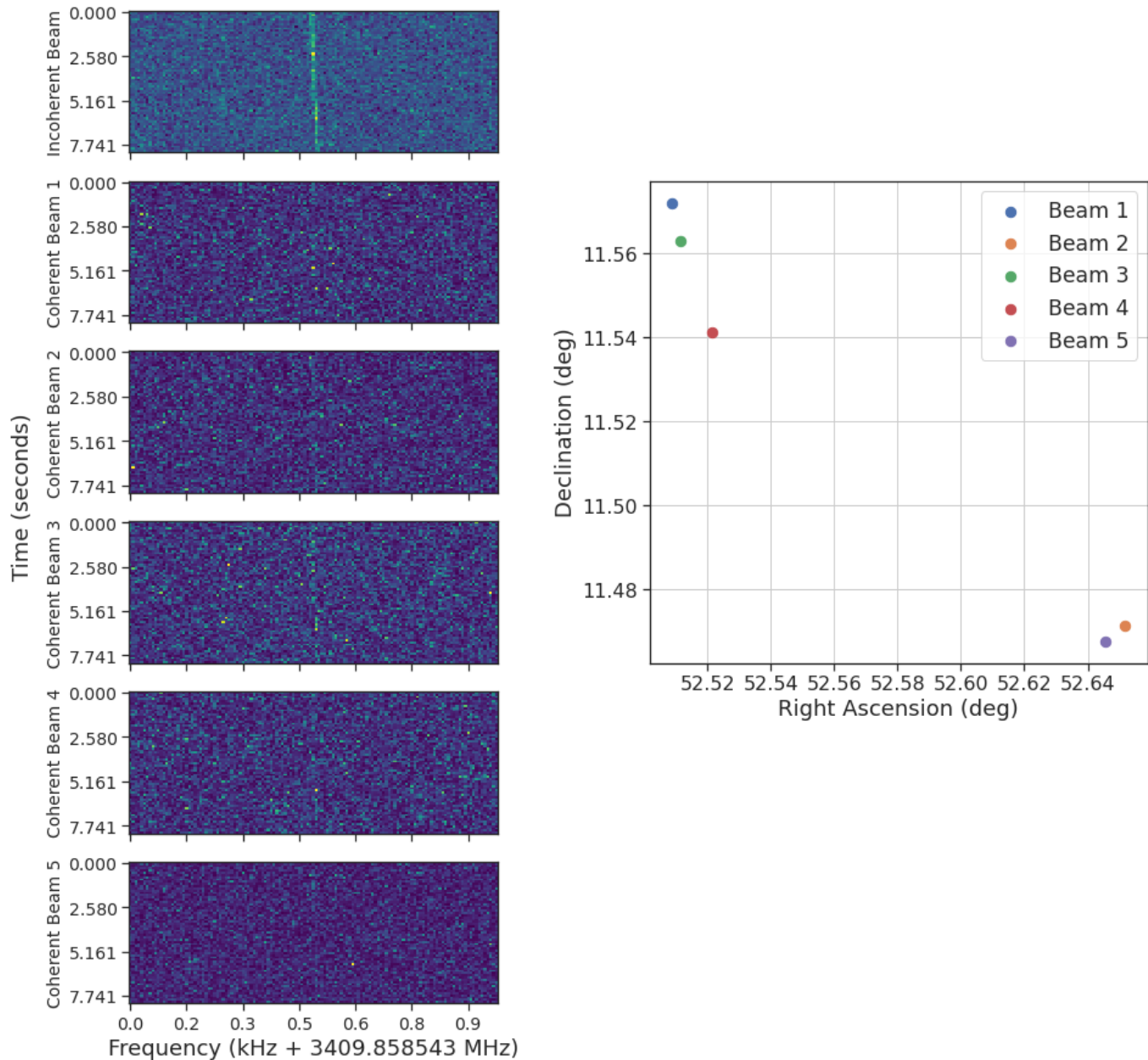


Figure 13. An example of the dynamic spectra from a single field in which the incoherent sum contained the main signal but the coherent beams each have a faint trace of the signal, indicating it is not likely an astronomical source of emission. All sources chosen are within the FWHM of the primary beam.

In this paper, we describe COSMIC’s operation relating to the observational strategy during the NRAO-hosted VLA all-sky survey, which observes the entire sky at declination’s above -40 degrees. The data are processed through an autonomous pipeline that generates a set of potential signals and logs the metadata into a MySQL database for scientists to filter through.

Using a test field of 30 minutes of data consisting of 511 sources, we describe a potential postprocessing pipeline that uses a series of filters to separate RFI from

signals with an astronomical origin. In this search, no potential technosignatures were identified. In the future, a faster and more automated version of this pipeline would allow for fast identification of potential candidates, which is a goal the team is striving toward.

This work overall represents an important milestone in our search. With the rapidly growing database, we need new methods for sorting through the data, and this paper describes a rapid and viable filtering mechanism.

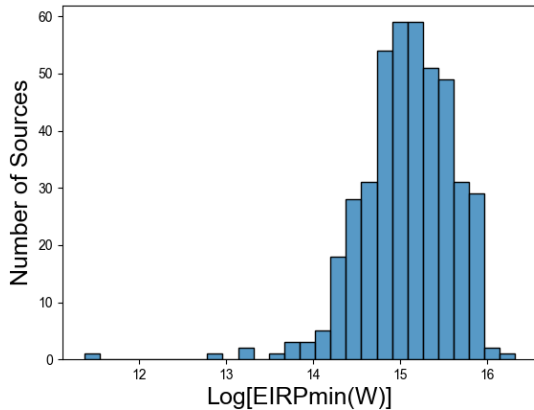


Figure 14. A plot showing the distribution of EIRP values calculated for each of the 511 sources evaluated during this work. The values range from 10^{11} to 10^{16} W, providing some of the lowest values for technosignatures to date.

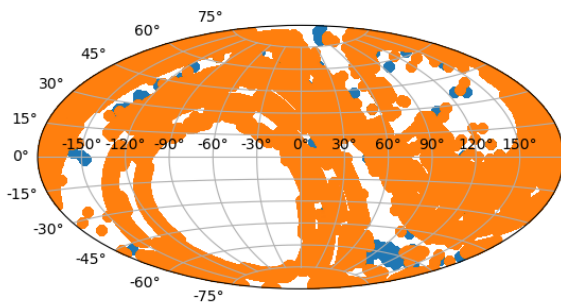


Figure 15. A plot in galactic coordinates of all the coordinates currently in the database observed from 29 March 2023 to 14 July 2024. The orange points represent data from frequencies below 4 GHz and the blue points are from data collected above 4 GHz.

Data Availability Statement—All software used in this publication is available on GitHub and is referenced throughout the paper. The observations using the COSMIC system on the VLA were collected during commensal observations and can be accessed by contacting the lead author on this team. If particular data or computing resources are needed, they can be provided by direct inquiry to the Breakthrough Listen team.

Software—

- TOPCAT – Taylor (2005)
- CASA – McMullin et al. (2007)
- NumPy v1.11.3 (Dubois et al. 1996), AstroPy (Astropy Collaboration et al. 2013), SciPy (Oliphant 2007), Matplotlib (Hunter 2007), Pandas (<https://pandas.pydata.org/docs/>)
- PYUVDATA – Hazelton et al. (2017)
- CARTA – Comrie et al. (2020)
- BLIMPY – <https://github.com/zoips/blimpy>
- ANSIBLE PLAYBOOK – <https://docs.ansible.com/>
- BLADE – <https://github.com/luigifcruz/blade>
- SETICORE – <https://github.com/lacker/seticore>
- HASHPIPE – MacMahon et al. (2018)
- xGPU – <https://github.com/GPU-correlators/xGPU>
- COSMIC Software – <https://github.com/COSMIC-SETI>
- target selector – <https://github.com/danielczech/targets-minimal>
- REDIS – <https://redis.com/>

We gratefully acknowledge the foundational support from John and Carol Giannandrea that has made COSMIC possible. We acknowledge additional support from other donors, including the Breakthrough Prize Foundation under the auspices of Breakthrough Listen. The National Radio Astronomy Observatory is a facility of the National Science Foundation operated under a cooperative agreement with Associated Universities, Inc. LS was funded as a participant in the Berkeley SETI Research Center Research Experience for Undergraduates Site, supported by the National Science Foundation under Grant No. 2244242. JS was funded by the NSF through the REU program at NRAO.

REFERENCES

- Astropy Collaboration, Robitaille, T. P., Tollerud, E. J., et al. 2013, *A&A*, 558, A33, doi: [10.1051/0004-6361/201322068](https://doi.org/10.1051/0004-6361/201322068)
- Briggs, F. H., Bell, J. F., & Kesteven, M. J. 2000, *The Astronomical Journal*, 120, 3351, doi: [10.1086/316861](https://doi.org/10.1086/316861)
- Choza, C., Bautista, D., Croft, S., et al. 2024, *AJ*, 167, 10, doi: [10.3847/1538-3881/acf576](https://doi.org/10.3847/1538-3881/acf576)

- Clark, M. A., LaPlante, P. C., & Greenhill, L. J. 2013, *International Journal of High Performance Computing Applications*, 27, 178, doi: [10.1177/1094342012444794](https://doi.org/10.1177/1094342012444794)
- Comrie, A., Wang, K.-S., Ford, P., et al. 2020, CARTA: The Cube Analysis and Rendering Tool for Astronomy, 1.3.0, Zenodo, doi: [10.5281/zenodo.3377984](https://doi.org/10.5281/zenodo.3377984)
- Czech, D., Isaacson, H., Pearce, L., et al. 2021, *PASP*, 133, 064502, doi: [10.1088/1538-3873/abf329](https://doi.org/10.1088/1538-3873/abf329)
- Dubois, P. F., Hinsen, K., & Hugunin, J. 1996, *Comput. Phys. Commun.*, 10, 262
- Ehman, J. 2008, The Big Ear Wow! Signal. <http://www.bigear.org/wow20th.htm>
- Enriquez, E., & Price, D. 2019, turboSETI: Python-based SETI search algorithm, *Astrophysics Source Code Library*, record ascl:1906.006. <http://ascl.net/1906.006>
- Etoka, S., Gray, M. D., & Fuller, G. A. 2012, *MNRAS*, 423, 647, doi: [10.1111/j.1365-2966.2012.20900.x](https://doi.org/10.1111/j.1365-2966.2012.20900.x)
- Gajjar, V., Perez, K. I., Siemion, A. P. V., et al. 2021, *AJ*, 162, 33, doi: [10.3847/1538-3881/abfd36](https://doi.org/10.3847/1538-3881/abfd36)
- Gray, M. 1999, *Philosophical Transactions: Mathematical, Physical and Engineering Sciences*, 357, 3277. <http://www.jstor.org/stable/1353849>
- Hazelton, B. J., Jacobs, D. C., Pober, J. C., & Beardsley, A. P. 2017, *The Journal of Open Source Software*, 2, 140, doi: [10.21105/joss.00140](https://doi.org/10.21105/joss.00140)
- Hickish, J., Beasley, T., Bower, G., et al. 2019, in *Bulletin of the American Astronomical Society*, Vol. 51, 269
- Houston, K. M. 2023, *Acta Astronautica*, 212, 505, doi: [10.1016/j.actaastro.2023.08.009](https://doi.org/10.1016/j.actaastro.2023.08.009)
- Huang, B.-L., Tao, Z.-Z., & Zhang, T.-J. 2023, *AJ*, 166, 245, doi: [10.3847/1538-3881/ad06b1](https://doi.org/10.3847/1538-3881/ad06b1)
- Hunter, J. D. 2007, *Comput. Sci. Eng.*, 9, 90, doi: [10.1109/MCSE.2007.55](https://doi.org/10.1109/MCSE.2007.55)
- Johnson, O. A., Gajjar, V., Keane, E. F., et al. 2023, *AJ*, 166, 193, doi: [10.3847/1538-3881/acf9f5](https://doi.org/10.3847/1538-3881/acf9f5)
- Lacy, M., Baum, S. A., Chandler, C. J., et al. 2020, *PASP*, 132, 035001, doi: [10.1088/1538-3873/ab63eb](https://doi.org/10.1088/1538-3873/ab63eb)
- Lacy, M., Baum, S. A., Chandler, C. J., et al. 2020, *Publications of the Astronomical Society of the Pacific*, 132, 035001, doi: [10.1088/1538-3873/ab63eb](https://doi.org/10.1088/1538-3873/ab63eb)
- Li, J.-K., Zhao, H.-C., Tao, Z.-Z., Zhang, T.-J., & Xiao-Hui, S. 2022, *ApJ*, 938, 1, doi: [10.3847/1538-4357/ac90bd](https://doi.org/10.3847/1538-4357/ac90bd)
- Li, M., & Margot, J.-L. 2024, in *American Astronomical Society Meeting Abstracts*, Vol. 243, American Astronomical Society Meeting Abstracts, 159.06
- Li, M. G., Sheikh, S. Z., Gilbertson, C., et al. 2023a, *AJ*, 166, 182, doi: [10.3847/1538-3881/acf83d](https://doi.org/10.3847/1538-3881/acf83d)
- . 2023b, *AJ*, 166, 182, doi: [10.3847/1538-3881/acf83d](https://doi.org/10.3847/1538-3881/acf83d)
- Ma, P. X., Ng, C., Rizk, L., et al. 2023a, *Nature Astronomy*, doi: [10.1038/s41550-022-01872-z](https://doi.org/10.1038/s41550-022-01872-z)
- . 2023b, *Nature Astronomy*, 7, 492, doi: [10.1038/s41550-022-01872-z](https://doi.org/10.1038/s41550-022-01872-z)
- MacMahon, D. H. E., Price, D. C., Lebofsky, M., et al. 2018, *PASP*, 130, 044502, doi: [10.1088/1538-3873/aa80d2](https://doi.org/10.1088/1538-3873/aa80d2)
- McMullin, J. P., Waters, B., Schiebel, D., Young, W., & Golap, K. 2007, in *Astronomical Society of the Pacific Conference Series*, Vol. 376, *Astronomical Data Analysis Software and Systems XVI*, ed. R. A. Shaw, F. Hill, & D. J. Bell, 127
- Méndez, A., Ortiz Ceballos, K., & Zuluaga, J. I. 2024, arXiv e-prints, arXiv:2408.08513, doi: [10.48550/arXiv.2408.08513](https://doi.org/10.48550/arXiv.2408.08513)
- Nita, G. M., & Gary, D. E. 2010, *MNRAS*, 406, L60, doi: [10.1111/j.1745-3933.2010.00882.x](https://doi.org/10.1111/j.1745-3933.2010.00882.x)
- Nita, G. M., Sadykov, V. M., Kosovichev, A. G., & Oria, V. 2019, in *AGU Fall Meeting Abstracts*, Vol. 2019, SH31E–3340
- Oliphant, T. E. 2007, *Comput. Sci. Eng.*, 9, 10, doi: [10.1109/MCSE.2007.58](https://doi.org/10.1109/MCSE.2007.58)
- Perley, R. 2016, *Jansky Very Large Array Primary Beam Characteristics*, Tech. rep., National Radio Astronomy Observatory (NRAO). https://library.nrao.edu/public/memos/evla/EVLAM_195.pdf
- Price, D. C., Enriquez, J. E., Brzycki, B., et al. 2020, *AJ*, 159, 86, doi: [10.3847/1538-3881/ab65f1](https://doi.org/10.3847/1538-3881/ab65f1)
- Sheikh, S. Z., Wright, J. T., Siemion, A., & Enriquez, J. E. 2019a, *ApJ*, 884, 14, doi: [10.3847/1538-4357/ab3fa8](https://doi.org/10.3847/1538-4357/ab3fa8)
- . 2019b, *ApJ*, 884, 14, doi: [10.3847/1538-4357/ab3fa8](https://doi.org/10.3847/1538-4357/ab3fa8)
- Sheikh, S. Z., Smith, S., Price, D. C., et al. 2021, *Nature Astronomy*, 5, 1153, doi: [10.1038/s41550-021-01508-8](https://doi.org/10.1038/s41550-021-01508-8)
- Siemion, A. P. V., Demorest, P., Korpela, E., et al. 2013, *ApJ*, 767, 94, doi: [10.1088/0004-637X/767/1/94](https://doi.org/10.1088/0004-637X/767/1/94)
- Smith, E., Lynch, R. S., & Pisano, D. J. 2022, *AJ*, 164, 123, doi: [10.3847/1538-3881/ac7e47](https://doi.org/10.3847/1538-3881/ac7e47)
- Smith, S., Price, D. C., Sheikh, S. Z., et al. 2021, *Nature Astronomy*, 5, 1148, doi: [10.1038/s41550-021-01479-w](https://doi.org/10.1038/s41550-021-01479-w)
- Tao, Z.-Z., Huang, B.-L., Luan, X.-H., et al. 2023, *AJ*, 166, 190, doi: [10.3847/1538-3881/acfc1e](https://doi.org/10.3847/1538-3881/acfc1e)
- Taylor, M. B. 2005, in *ASP Conference Series*, Vol. 347, *Astronomical Data Analysis Software and Systems XIV*, ed. P. Shopbell, M. Britton, & R. Ebert, 29
- Tremblay, C. D., Varghese, S. S., Hickish, J., et al. 2024, *AJ*, 167, 35, doi: [10.3847/1538-3881/ad0fe0](https://doi.org/10.3847/1538-3881/ad0fe0)
- Wang, Y.-C., Tao, Z.-Z., Zhang, Z.-S., et al. 2023, *AJ*, 166, 146, doi: [10.3847/1538-3881/acf12a](https://doi.org/10.3847/1538-3881/acf12a)
- Weber, R., Faye, C., Biraud, F., & Dansou, J. 1997, *Astron. Astrophys. Suppl. Ser.*, 126, 161, doi: [10.1051/aas:1997257](https://doi.org/10.1051/aas:1997257)

Wolfe, J. H., Billingham, J., Edelson, R. E., et al. 1981, in
NASA Conference Publication, Vol. 2156, NASA
Conference Publication, ed. J. Billingham, 391
Wright, J. T., Kanodia, S., & Lubar, E. 2018, The
Astronomical Journal, 156, 260,
doi: [10.3847/1538-3881/aae099](https://doi.org/10.3847/1538-3881/aae099)

Zhang, Z.-S., Werthimer, D., Zhang, T.-J., et al. 2020, ApJ,
891, 174, doi: [10.3847/1538-4357/ab7376](https://doi.org/10.3847/1538-4357/ab7376)